Synthetic Metals, *59* (1993) 279–295

Characterization of fullerenes and doped fullerenes

C. S. Yannoni, H. R. Wendt, M. S. de Vries, R. L. Siemens, J. R. Salem, J. Lyerla, R. D. Johnson, M. Hoinkis, M. S. Crowder, C. A. Brown and D. S. Bethune

IBM Research Division, Almaden Research Center, 650 Harry Road, San Jose, CA 95120-6099 (USA)

L. Taylor, D. Nguyen, P. Jedrzejewski and H. C. Dorn

Department of Chemistry, Virginia Polytechnic University, Blacksburg, VA 24061 (USA)

Abstract

The results of a variety of experiments used to characterize fullerenes, metallofullerenes and alkali-metal intercalated C_{60} are reported. It is shown that differential scanning calorimetry and NMR characterization of the orientational phase transition in C_{60} provide sensitive means to assess the purity and crystallinity of fullerene samples. The results of a mass-spectrometric investigation of metallofullerene samples produced by co-vaporization of carbon and metals are described. An account is given of some electron paramagnetic resonance results obtained for LaC_{82} and solid-state NMR results obtained on an alkali-intercalated fullerite, Rb_3C_{60}, which show for the first time the presence of magnetically inequivalent carbons in underivatized C_{60}. Together these experiments yield a great deal of information about the phase purity, molecular dynamics and structure of a variety of fullerene materials.

1. Introduction

We report here the results of a variety of experiments that we have used to characterize fullerenes, metallofullerenes and alkali-metal intercalated C_{60}. In Section 2 it is shown that differential scanning calorimetry (DSC) and NMR characterization of the orientational phase transition in C_{60} provide sensitive means to assess the purity and crystallinity of fullerene samples. In Section 3 the results of a mass-spectrometric investigation of metallofullerene samples produced by co-vaporization of carbon and metals are described. Section 4 gives an account of some electron paramagnetic resonance results obtained for LaC_{82} and, finally, Section 5 presents solid-state NMR results obtained on an alkali-intercalated fulleride, Rb_3C_{60}, which show for the first time the presence of magnetically inequivalent carbons in underivatized C_{60}. Together these experiments yield a great deal of information about the phase purity, molecular dynamics and structure of a variety of fullerene materials.

2. DSC and NMR characterization of the orientational phase transition in C_{60}

The orientational phase transition near 260 K, observed in C_{60} by differential scanning calorimetry (DSC) [1, 2] and X-ray diffraction [3] has subsequently been studied extensively using ^{13}C NMR [4–6], X-ray diffraction [7], neutron scattering [8–12], muon spin-rotation (μSR) [13], Raman spectroscopy [14, 15] and ultrasonic techniques [16]. Even though the phase transition is sensitive to the purity and the degree of crystalline perfection of the sample, with a few exceptions [14–16], measurements to date have been carried out on powder samples with significant levels of impurities and defects. To improve the precision of such experiments will require the use of samples of higher quality, making it important to have convenient techniques for assessing sample purity and crystallinity.

We have used DSC to characterize C_{60} samples prepared in various ways, a sample of purified C_{70} and a mixture of C_{60} with C_{70}. The results dramatically illustrate the ability of this technique to detect sensitively the changes in orientational phase transition and confirm its utility as a means to characterize these materials [1, 2]. Data characterizing the phase transition in C_{60} were also obtained using ^{13}C NMR, which showed changes in the transition temperature and width which paralleled the results of the DSC measurements. Crystals grown by vacuum sublimation of C_{60} are found to give extremely clean, sharp DSC isotherms and the highest transition temperature observed. For this sample NMR gave a transition width of less than 1 K and a transition temperature in agreement with that obtained by DSC.

DSC measurements were made using a DuPont 910 DSC with a 2100 controller, with the heating rate set at 20 °C/min. Sample sizes ranged from 3 to 20 mg, depending upon availability. DSC curves were obtained on six different samples:

Sample 1 (toluene extract) — A sample of fullerene-containing soot was prepared in the manner previously described [17] and was extracted with toluene. The extract contained 85% C_{60}, 15% C_{70} and traces of higher fullerenes.

Samples 2 and 3 (chromatographically purified C_{60} and C_{70}) — The above extract was then separated using liquid chromatography (basic alumina) with a solvent system of 95/5 hexane/toluene as recently described by Diederich *et al.* [18]. Portions of the chromatographically purified C_{60} fraction were further treated to give purified samples as follows:

Sample 4 (supercritical CO_2-washed C_{60}) — Purified C_{60} was continuously extracted for 3 h with supercritical CO_2 (70 °C) in an attempt to reduce the level of solvents (e.g. toluene) present in the sample.

Sample 5 (CO_2-washed and heated C_{60}) — A portion of sample 4 was further purified by heating in a 1.3×10^{-5} Pa (10^{-7} Torr) vacuum for 2 h at 200 °C. Gas evolution was readily observed during this vacuum heating procedure.

Sample 6 (vapor-grown crystals of C_{60}) — Chromatographically purified C_{60} was heated in a quartz tube at 1.3×10^{-5} Pa vacuum for 12 h at 200 °C to drive off solvents. The temperature was then gradually raised to 450 °C, subliming material over to another portion of the tube. That portion was pinched off and placed in a temperature gradient with one end at about 650 °C and the other at about 500 °C for 2 h. Crystals formed at the cool end in clumps, with individual crystals typically 100 μm in size. Laser-desorption/laser-ionization mass spectrometry of crystals formed in this way showed only the presence of C_{60}.

Figure 1 shows the endotherm obtained from sample 6, the vapor-grown C_{60} crystal sample. The transition gives a single, clean, very narrow endotherm (FWHM = 2.8 K), with an extrapolated onset temperature of 262 K, a peak at 264 ± 1 K and no identifiable shoulders or multiple peaks. Such an endotherm indicates that this sample has a very high degree of purity and crystallinity. The curve is similar to those reported previously by Dworkin *et al.* [1, 2] and Heiney *et al.* [3] but shows somewhat greater symmetry. In our case, the portion of the curve at temperatures below the transition is slightly displaced in the endothermic direction (downward) compared to the portion above the transition. The peak minimum and extrapolated onset temperature in Fig. 1 appear to be approximately 4 K higher than the corresponding points in refs. 1–3, and the measured enthalpy change is 6620 J/mol, significantly higher than found in the previous measurements. NMR measurements made on sample 6 showed a phase transition at the same temperature as found by DSC. The width of the endotherm peak for this sample is comparable to that found for a fast melting, high purity indium melting-point standard run at the same heating rate, confirming that this is high-purity material with a very narrow distribution of transition temperatures.

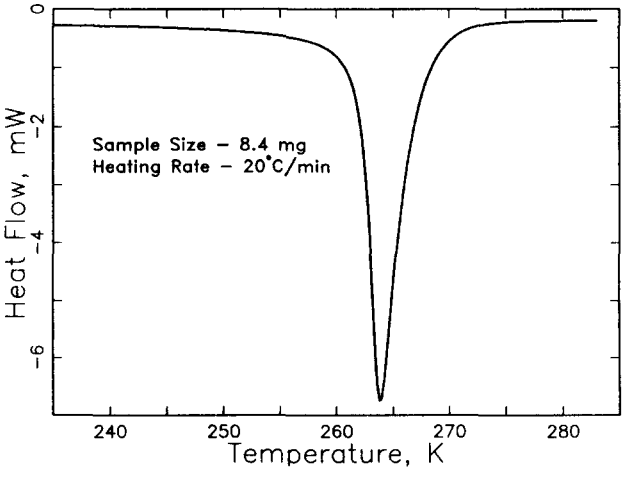

Fig. 1. DSC curve of C_{60} crystals grown from vapor phase-sublimed material (sample 6). The endotherm has a FWHM of 2.8 K.

Markedly different results are obtained with samples of lesser purity and crystalline order, as will be described below.

DSC results for sample 4, which was cleaned by supercritical CO_2 extraction, are shown in Fig. 2(a). The trace shows two incompletely separated endotherms with a total enthalpy change of 4320 J/g. Figure 2(b) shows a second DSC trace for the same sample, after the sample was heated to 250 °C in the course of the first run. The endotherm has changed substantially. The lower temperature peak has diminished in size and moved to higher temperature, while the higher temperature peak has grown and sharpened. A curve very similar to that in Fig. 2(b) is obtained for sample 5 (shown in Fig. 2(c)), from which most of the CO_2 had presumably been removed by heating in vacuum prior to the DSC measurement. This suggests that the lower temperature peak is related to the presence of CO_2, introduced by the supercritical CO_2 extraction. It is apparent that CO_2 incorporated in the sample greatly affects the endotherm obtained and, furthermore, that it is not easily removed by subsequent heating (compare Fig. 1 and Figs. 2(b) and (c)).

Figure 3 shows the results of NMR relaxation experiments on the vapor-grown crystal sample 6 and the supercritically cleaned and heated sample 5, at 254 K (below the order–disorder phase transition). The slopes of the ^{13}C magnetization recovery curves allow a sensitive determination of the rotational correlation time of C_{60} [5]. For sample 6, the recovery curve is characterized by a single exponential (Fig. 3(a)), which indicates that the molecules in the sample have a uniform rotational correlation time; we note that this time is 30 times longer for molecules in the ratchet phase (just below the phase transition temperature) where the molecules rotate by

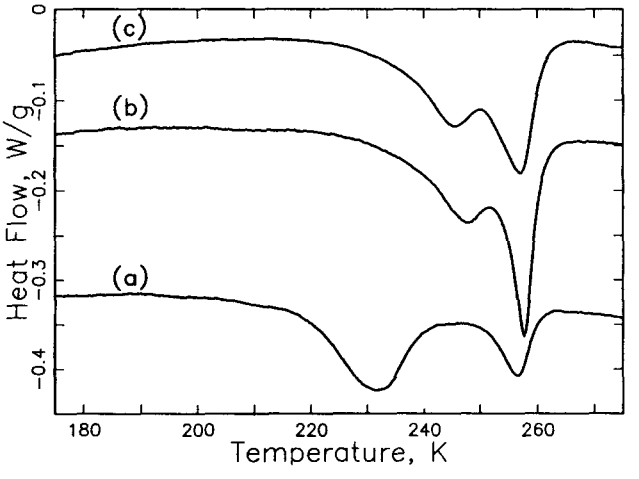

Fig. 2. DSC curves: (a) sample 4, the CO_2 extracted sample of chromatographically purified C_{60} as received; (b) sample 4, second run (the sample had been heated to 250 °C in the course of the first run); (c) sample 5, as in (a), but heated in vacuum prior to the DSC measurement, as described in the text.

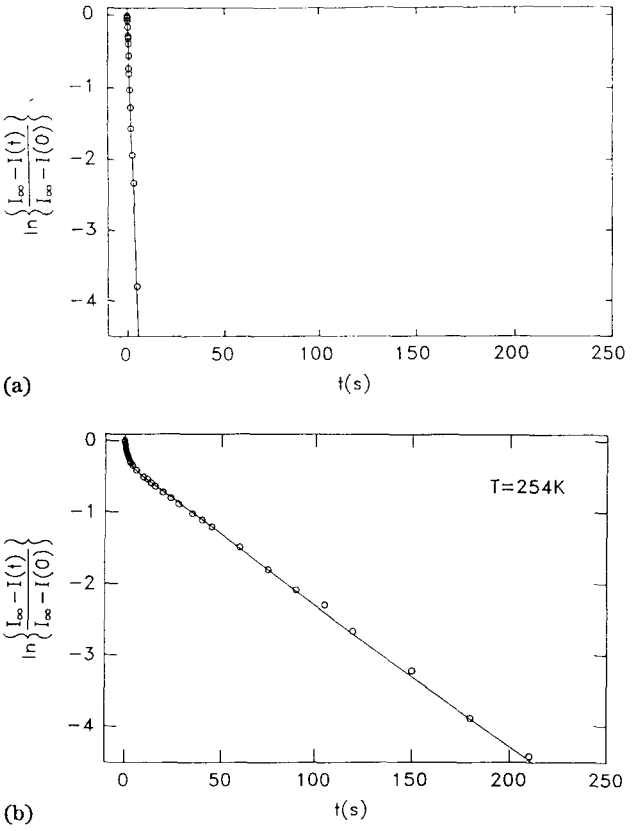

Fig. 3. Log plots of intensity data from inversion recovery experiments on C_{60} at 254 K: (a) vapor-grown C_{60} crystals (sample 6); (b) supercritically cleaned and heated C_{60} (sample 5). While both samples are below their phase transition temperatures (262 and 258 K, respectively), the single-component decay for the crystal (sample 6) shows it to be uniformly in the 'ratchet' phase, while sample 5 shows two-component behavior, with a substantial fraction of the sample still in the 'rotator' phase.

symmetry equivalent jumps [3–5] than it is in the rotator phase (just above the transition). This transition in sample 6, as seen by NMR, has a width of less than 1 deg. and may be limited by thermal gradients in the sample. In contrast, the recovery data for sample 5 (Fig. 3(b)) show two distinct components: a rapidly decaying component characteristic of the ratchet phase and a more slowly decaying component, the recovery rate of which is indicative of the very rapid rotations found in the disordered high-temperature 'rotator' phase [5]. NMR relaxation experiments indicate that rotation of C_{60} in the rotator phase occurs at the same rate for both the vapor-grown crystal (sample 1) and the supercritically cleaned and heated sample 5; rotation in the ratchet phase is significantly slower for the crystal sample [19]. Figure 4 shows the results obtained for sample 2, consisting of chromatographically purified C_{60} which has been dried (but not CO_2-extracted). This sample also gives a curve showing a sharp peak with a shoulder. The shoulder most

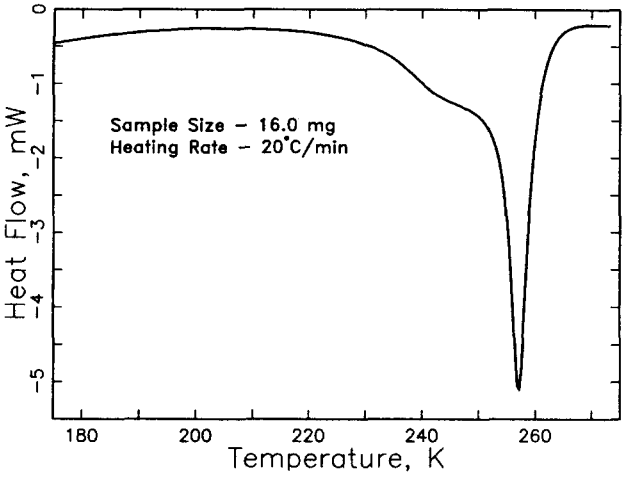

Fig. 4. DSC curve for sample 2, chromatographically purified C_{60}.

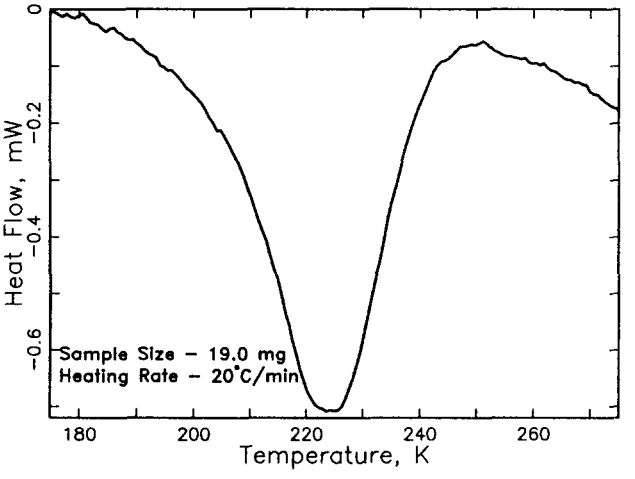

Fig. 5. DSC curve for sample 1, toluene extract, showing the small, broad endotherm.

likely is a consequence of the presence of residual solvents incorporated in the lattice. Comparison of this curve with those shown in Fig. 2 provides convincing evidence that CO_2 extraction introduces a substantial amount of CO_2 into the sample.

Finally, the results obtained for the toluene extract of the soot (sample 1) are shown in Fig. 5. In this case a very broad endotherm is obtained ($\sim$22 K), with an enthalpy change on the order of 2 J/g. An endotherm having such a large width and small ΔH is near the limit of the measurement capability of our instrument. The broad distribution of transition temperatures may reflect disruption of the crystal ordering due to the random inclusion of C_{70} molecules (which comprise about 15% of the sample). This idea is supported by the fact that the curve for sample 2 (the purified C_{60} fraction)

shows a relatively sharp endotherm compared to the C_{60}/C_{70} mixture. The characteristics of sample 2, with an endotherm minimum at 257 K and a ΔH value of 8.2 J/g, are much closer to those of the vapor-grown crystal. Incorporation of solvent into the solid is also likely to account for part of the broadening of the transition in the toluene extract (sample 1), but comparison with sample 2 leads us to conclude that this is less important than the presence of C_{70}.

The chromatographically purified C_{70} fraction (sample 3) shows no detectable transitions, nor does the soot from which these fullerenes were separated using the same DSC conditions. Two transitions have been reported for C_{70} (at 276 and 337 K) by Vaughan *et al.* [20] in samples which were sublimed to remove any solvents.

We conclude that DSC measurements of the characteristics of the orientational phase transition in solid C_{60} provide a convenient diagnostic technique which is sensitive to both the presence of impurities, such as solvents and CO_2, and to crystal defects, in agreement with the findings of Dworkin *et al.* [1, 2]. The DSC endothermic transitions observed correlate well with the results of NMR experiments. It seems clear that these techniques will also be applicable to other fullerene solids.

3. Laser-desorption/laser-ionization mass spectrometry of metallofullerenes

Metallofullerenes prepared by arc vaporization of either specially prepared composite carbon/metal rods [21, 22] or cored carbon rods packed with mixtures of graphite and metal powders [23] have been analyzed by laser-desorption/laser-ionization mass spectrometry. In this section a number of issues relating to this analysis will be addressed. First, it will be shown that the metallofullerene complexes are not formed in the laser desorption step itself, but rather are present in the bulk material on the surface, prior to analysis. It can also be shown that laser desorption can be used to vaporize metallofullerenes that decompose upon slower heating. The second step in the analysis is photoionization and its merits will be discussed. Finally, some emerging trends concerning metallofullerenes with Group IIIB elements will be pointed out.

These experiments were carried out in a laser desorption jet cooling apparatus described earlier [24]. Essentially, molecules on a surface are laser-desorbed, entrained in an Ar supersonic expansion and detected downstream by (multi)photon ionization and time-of-flight mass spectrometry. Desorption was performed with either 532 nm light from a doubled Nd:YAG laser or with 248 nm light from a KrF excimer laser. No difference was observed. Ionization was achieved with 193 nm excimer laser radiation. In principle it is possible to form van der Waals complexes, both in the desorption step and in the supersonic expansion. Since it is conceivable that both metals and fullerenes could be present on the surface separately, it is important to

prove that the observed metallofullerenes are not formed by complex formation during the analysis. Figure 6 shows a mass spectrum obtained from a sample that contained a dried toluene extract of a mixture of (a) lanthanum-containing soot and (b) soot that was produced without lanthanum from ^{13}C-enriched graphite. Clearly both soot (a) and soot (b) contain C_{60} as well as C_{70}; however, only soot (a) contains a metallofullerene, LaC_{82}. If this species had been produced by desorption or jet cooling, then we would have also observed the ^{13}C-enriched metallofullerene. This demonstrates that the metallofullerene is present on the surface, prior to analysis.

Generally, laser desorption can be used for analysis of organics that are unstable upon heating, because, with a laser pulse duration of the order of nanoseconds, compounds can be volatilized while avoiding thermochemical decomposition [25]. In the case of fullerenes that advantage is not always crucial, since these species appear to be quite stable upon heating. However, for some metallofullerenes, laser desorption may be essential. A case in point is provided by various metallo-C_{60} and metallo-C_{70} species. Figure 7(a) shows a laser-desorption mass spectrum of arc soot from composite rods containing gadolinium in addition to carbon. As can be seen, the dominant species in the spectrum is GdC_{60}, followed by GdC_{70}. In various experiments the soot was heated, in either stainless steel or quartz ovens, in vacuum, to various temperatures ranging from 300 to 700 °C. It was found that stable metallofullerenes sublime at temperatures comparable to the bare fullerene analogs.

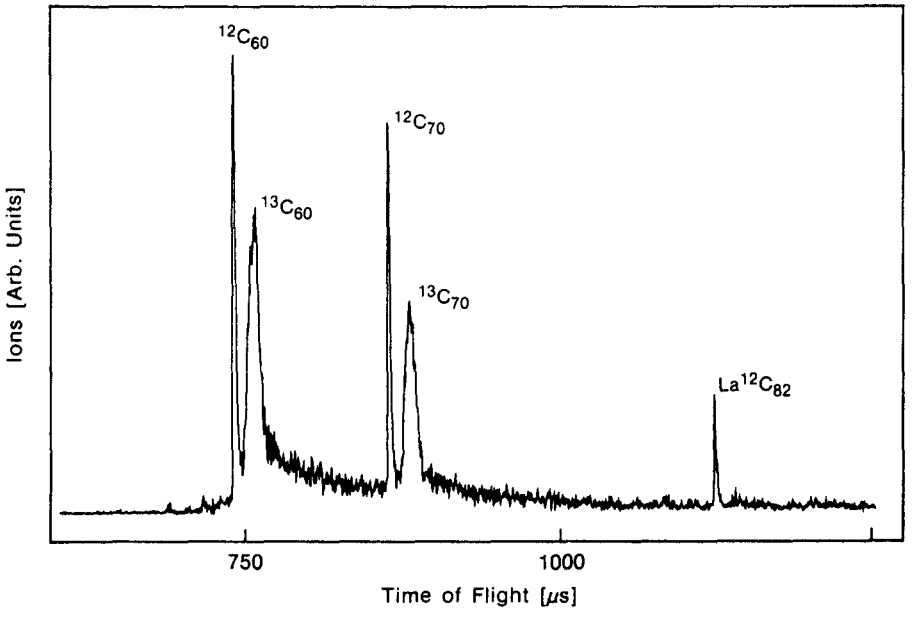

Fig. 6. Laser-desorption/laser-ionization time-of-flight mass spectrum obtained from dried toluene extract of a mixture of lanthanum-containing soot and soot that was produced without lanthanum from ^{13}C graphite. The peaks labeled as ^{13}C show the envelope of the mass distribution, corresponding to an enrichment of about 20%.

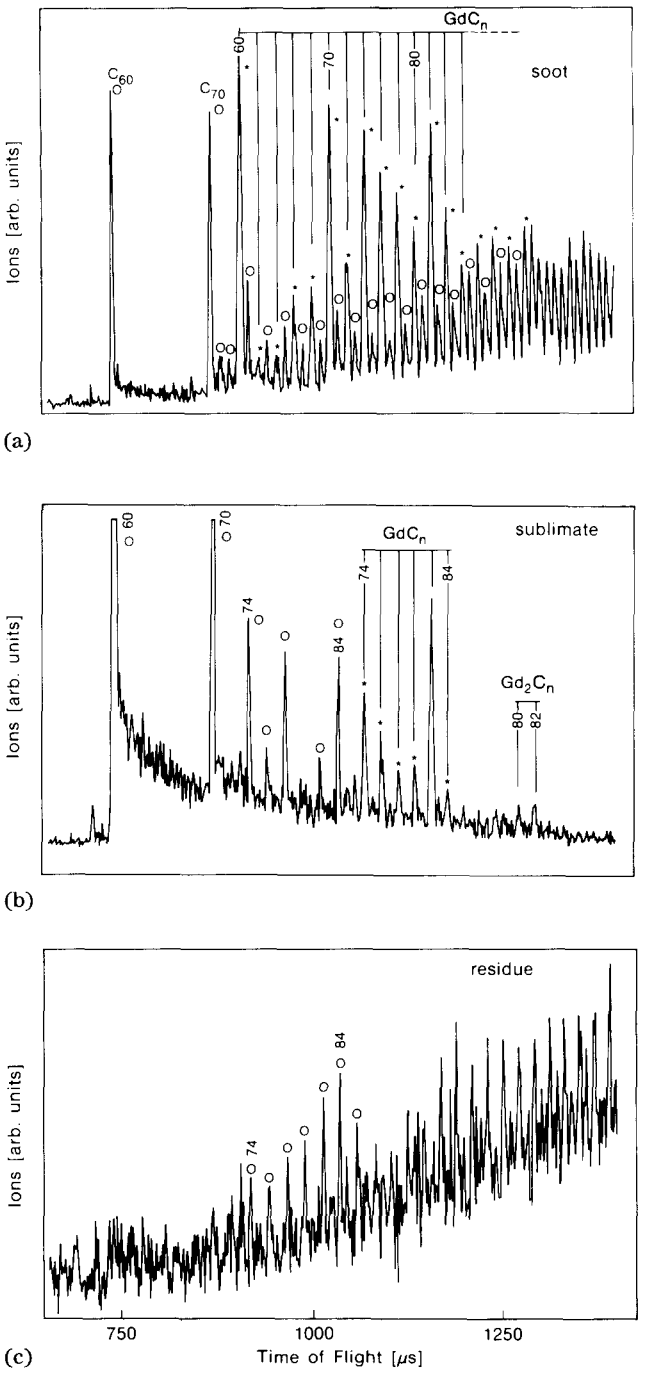

Fig. 7. Laser-desorption/laser-ionization time-of-flight mass spectra of carbon arc soot in which gadolinium was added to the electrode rods: (a) untreated soot; (b) material that was vacuum sublimed from the soot at 650 °C; (c) shows the spectrum of the residue after sublimation. Desorption is with 532 nm, ionization with 193 nm.

In other words, the sublimation temperature increases with number of carbons and is not significantly affected by the metal; however, the lighter metallofullerenes, such as the C_{60} and C_{70} species, are decidedly unstable. Figure 7(c) shows a mass spectrum of the soot after heating, while Fig. 7(b) shows a mass spectrum of the sublimed material. It appears that the species that are dominant in the spectra of the unheated soot decompose or otherwise react upon slow heating; however, they can be volatilized by rapid laser heating. It is noteworthy that the least stable metallofullerenes are those formed with the most stable bare fullerenes. Along the same lines it is noted that toluene extraction, which is very selective for C_{60} and C_{70}, shows a remarkably different selectivity for the metallofullerenes. Generally, toluene extraction yields predominantly the metallo-C_{82} species. The solubility of these species in toluene is less than that for bare C_{60} and bare C_{70}, but significantly more than that for other metallofullerenes.

Table 1 gives the predominant species that result from toluene extraction of metallofullerene-containing soot, as determined by two-laser mass spectrometry. The trivalent ionic radii of the metals are given as well. The trend of the data indicates that more multiple-metal species form as the ionic radius decreases. Sc_2C_n species are observed with n ranging from 80 to 90 (even numbers only) with peak heights of the same order of magnitude. Mono-scandium and tri-scandium metallofullerenes are observed by EPR spectroscopy [23, 27] and in the mass spectra as well, but with at least an order of magnitude less intensity than di-scandium species.

Finally, it needs to be pointed out that care should be exercised in interpreting photoionization mass spectra, since relative ionization efficiencies are unknown. In the case of bare C_{60} the ionization potential is higher than the photon energy and 193 nm photons excite the molecule to a very short-lived state, which intersystem crosses to a low-lying triplet state at about 1.6 eV [28]. The molecule is subsequently one- or two-photon ionized from this state. For metallofullerenes, both the ionization potential and the electronic spectroscopy could be different from empty fullerenes. In the extreme case of a sufficiently lowered ionization potential, some of these molecules could

TABLE 1

Dominant species in toluene extracts of metallofullerene soot

M	MC_{82}	M_2C_{82}	Radius[a]
Sc		X[b]	0.732
Er	X	X	0.881
Y	X	X	0.893
Tb	X		0.923
Gd	X		0.938
La	X		1.06

[a]Crystal ionic radii (in Å) of trivalent metals from ref. 26.

[b]Di-scandium fullerenes with 80, 82 and 84 carbon atoms have about equal abundance. At slightly lower abundance di-scandium fullerenes are observed with up to 100 carbon atoms.

even be single-photon ionized at 193 nm. For LaC_{82}, comparison with XPS measurements shows the photoionization detection to be greater in efficiency than that of bare C_{60} and C_{70}.

4. Electron paramagnetic resonance of lanthanum-fullerenes

Evidence that metal atoms can combine with arc-vaporized carbon atoms to form metallofullerene molecules [29] was reported shortly after the discovery of fullerene molecules [30]. More recently, correlative mass spectroscopic (MS) and electron paramagnetic resonance (EPR) studies have identified the metallofullerenes LaC_{82} [22], YC_{82} [31] and Sc_3C_{82} and ScC_{82} [23, 27]. Thus, mass spectrometry has been used to identify these novel molecules while EPR has provided the first detailed information regarding their electronic ground states. In this section, EPR multiplets of La fullerene molecules will be examined in detail with the intent of underlining the delocalized nature of their paramagnetic ground states.

Samples were prepared by toluene extraction of soot produced from arc-burning of either composite graphite–metal oxide rods [21, 22] or cored carbon rods packed with mixtures of graphite and metal powders [23]. For EPR study the toluene extract was transferred to a quartz tube, degassed by the freeze-pump-thaw method and vacuum sealed. A Bruker ER300 X-band EPR spectrometer was used to record the spectra.

Figure 8(a) displays an experimental room-temperature X-band (9.7 GHz) EPR spectrum of the toluene extract while Fig. 8(b) shows a simulated spectrum composed of two overlapping eight-line patterns (octets). Both octets, arising from electron hyperfine coupling to the lanthanum nuclear spin ($I = 7/2$), were generated with the parameters listed in Table 2. The g

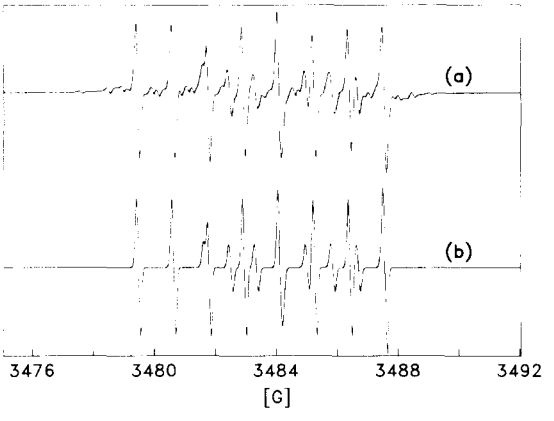

Fig. 8. (a) Experimental room-temperature X-band (9.7 GHz) EPR spectrum of the toluene extract. (b) Simulated spectrum composed of two overlapping eight-line patterns (octets). The octets arise from electron hyperfine coupling to the lanthanum nuclear spin ($I = 7/2$). The simulation parameters are listed in Table 2.

TABLE 2

Parameters used to fit two octets to the EPR spectrum of LaC_{82}

Octuplet no.	g value	A (G)	ΔH_{pp}	Rel. intensity
1	2.0009	1.15	0.12	3
2	1.9989	0.83	0.13	1

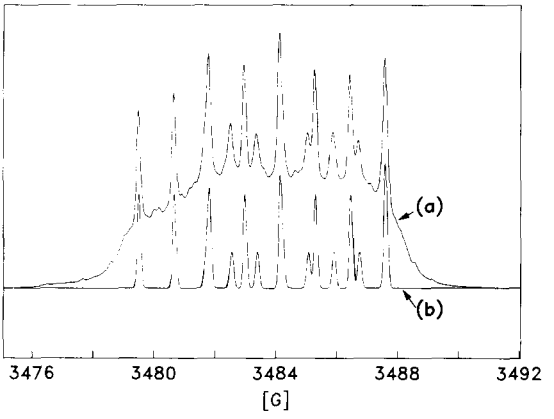

Fig. 9. Integrals of (a) experimental and (b) simulated spectra shown in Figs. 8(a) and (b), respectively. Notice the broad absorption background in (a), the integration of the experimental spectrum (Fig. 8(a)).

value and hyperfine coupling for octet no. 1 are the same as those reported for LaC_{82} [22], while the second octet spectrum (no. 2) has not been reported previously. The mass spectrum of this sample shows only one peak corresponding to LaC_{82}. The observation of a single peak in the mass spectrum and two EPR octets suggests that the EPR spectra are due to conformers of the same metallofullerene.

Figures 9(a) and (b) are the integrals of the experimental and simulated spectra shown in Figs. 8(a) and (b), respectively. The most striking feature in Fig. 9 is the broad absorption background obtained from integration of the experimental spectrum (Fig. 8(a)), which is absent in the integral of the spectrum simulated with the parameters given in Table 2 (Fig. 9(b)). The origin of this broad background signal can be traced to the experimental spectrum taken in the derivative mode, where small unresolvable features flank the high-intensity lines comprising the octets. We propose that the broad background absorption of Fig. 9(a) is due to unresolved electron–nuclear hyperfine coupling with naturally abundant (1.1%) ^{13}C spins in the fullerene cage [22]. This interpretation is supported by statistics of the percentage of LaC_{82} species which contain no ^{13}C atoms. For an ensemble of C_{82} fullerenes, 40% contain only ^{12}C atoms, while the remaining 60% have one or more ^{13}C atoms. Simulation of the derivative spectrum (Fig. 8(b)) appears

to match the experimental spectrum quite well, but does not include ^{13}C hyperfine interactions. Assuming that fullerenes which contain one or more ^{13}C atoms do not contribute to the sharp octet spectra shown in Fig. 8(a), i.e., that there are no ^{13}C hyperfine splittings less than the width of the lines in the octet spectrum ($\sim$60 mG), the simulated spectrum (Fig. 8(b)) should faithfully reflect the signal intensity only from lanthanum-fullerene species which contain only ^{12}C atoms (40% of the total absorption). Therefore, the area under the absorption curve of Fig. 9(b) should be 40% of the total absorption intensity for all lanthanum-fullerene species given by the area under the experimental absorption spectrum (Fig. 9(a)). We find that the ^{12}C-only species account for only 14% of the total spectral intensity. Despite this discrepancy, possibly due to the high sensitivity of a double-integration to the wings of the line [32] or an impurity resonance, the majority of the absorption (i.e., the broad background absorption) is associated with lanthanum-fullerenes which contain one or more ^{13}C atoms. This finding is consistent with the small value of the ^{139}La hyperfine couplings given in Table 2. A theoretical calculation of the isotropic hyperfine splitting for La^{+2} yields a value of 186 G, almost two orders of magnitude greater than our experimentally determined value*. Thus, less than 1% of the unpaired electron spin density is localized at the lanthanum atom, the rest being distributed over the carbon atoms on the fullerene shell, and the lanthanum is best described as a +3 cation. This is consistent with an earlier calculation for LaC_{60}, which found a net lanthanum charge of $+2.85e$ [34].

Further experiments are in progress to characterize more quantitatively the nature of the paramagnetic ground state of lanthanum-fullerene complexes.

5. High-resolution low-temperature NMR spectra of conducting alkali-metal-doped fullerides

One of the most exciting developments in fullerene research has been the discovery that the alkali-metal-doped fullerenes M_3C_{60} are conductors as well as superconductors at relatively high temperatures [35, 36]. A number of structural studies have been made which show that the C_{60} units are arranged in the lattice in much the same way as in the pure undoped material and that the alkali metal atoms are interspersed between the C_{60} units in interstitial sites [37, 38]. ^{13}C NMR studies have proved to be very powerful in probing the conducting state in both K_3C_{60} [39] and $KTl_{1.5}C_{60}$ [40]. We report here the results of variable-temperature magic-angle spinning (MAS) ^{13}C NMR experiments on Rb_3C_{60} and the first resolution of individual chemical shifts for the carbon atoms on $C_{60}{}^{-3}$, an unsubstituted C_{60} species.

*If we assume that the lanthanum is in a zero-valence state, the calculated hyperfine coupling is 2137 G (see ref. 33), which means that only 0.05% of the unpaired electron spin density is localized on the lanthanum atom in LaC_{82}.

The Rb-doped material was made according to the method described by McCauley *et al.* [41]. In brief, chromatographically purified [18] C_{60} was dried for 24 h under vacuum at 225 °C and then heated with excess rubidium (225 °C) in a sealed, evacuated, Pyrex tube for 24 h to produce Rb_6C_{60}. This material was mixed in a glove box (under argon) with 1.2 times the initial amount of C_{60}, resealed in a Pyrex tube and heated successively to 250 °C (24 h), 350 °C (24 h) and finally to 450 °C (1 h) to produce Rb_3C_{60}. The doped powder was packed into a 5 mm thin-wall NMR tube in a dry box and sealed under vacuum. Low-temperature ^{13}C MAS spectra were obtained on a home-built probe at 1.4 T field strength (15 MHz ^{13}C operating frequency) [42].

^{13}C MAS spectra of Rb_3C_{60} at several temperatures are shown in Fig. 10. A spectrum of undoped C_{60} (143 ppm) [43] is shown in Fig. 10(a) for reference. At ambient temperature, the Rb-doped material also yields a single, narrow line shifted 43 ppm downfield from undoped C_{60} (Fig. 10(b)). The

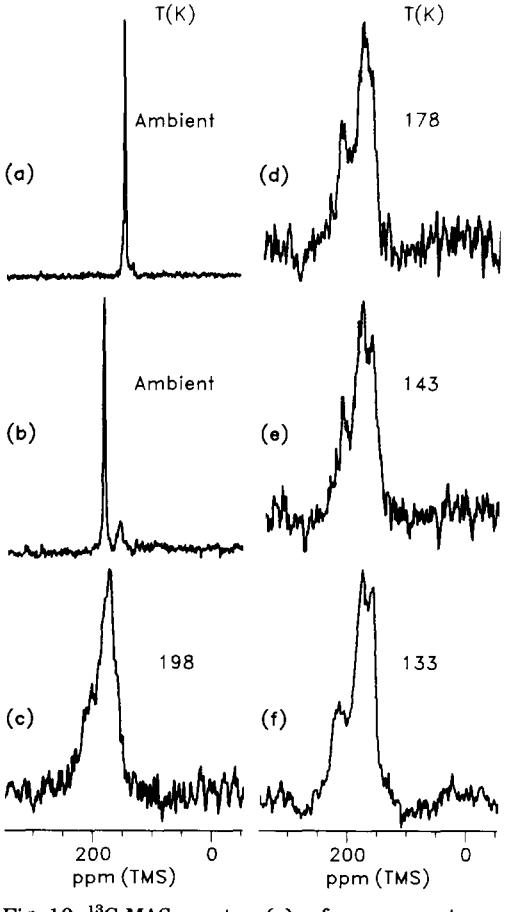

Fig. 10. ^{13}C MAS spectra: (a) reference spectrum of undoped C_{60} taken at ambient temperature; Rb_3C_{60} at (b) ambient temperature; (c) 198 K; (d) 178 K; (e) 143 K; and (f) 133 K.

resonance at 157 ppm appears to be due to an impurity. As the temperature is lowered, the chemical shift remains constant, but the line broadens, developing a pronounced downfield shoulder, as well as a hint of an upfield shoulder (Fig. 10(c)). At 178 K (Fig. 10(d)), the downfield shoulder has moved farther downfield and has sharpened into a peak at 214 ppm, while the upfield shoulder has increased in intensity. At the lowest temperatures shown, 143 and 133 K (Figs. 10(e) and (f)), the upfield band has split into two peaks at 176 and 159 ppm. No further changes are observed as the temperature is lowered to 77 K. The low-temperature-limit ^{13}C MAS NMR spectrum of Rb_3C_{60}, which shows three peaks, indicates that there are carbons in three different environments in the C_{60}^{-3} sub-units. The data reported here are thus the first detection of magnetically inequivalent carbons in an unsubstituted C_{60} moiety. These results appear to be consistent with the X-ray structure of Rb_3C_{60} [14] since examination of that structure reveals that there are carbons in three different environments.

The X-ray study also shows that the C_{60} units are orientationally ordered at room temperature with a random distribution between two orientations and it was suggested that the Rb atoms may inhibit rotation of the fullerenes [38]. Nonetheless, the NMR lineshape changes shown in Fig. 10 are diagnostic for rapid reorientation of the C_{60}^{-3} units. Clearly, the room-temperature ^{13}C spectrum in Fig. 10(b) shows averaging of the three different isotropic chemical shifts resolved in the low-temperature spectra and the temperature dependence of the NMR spectra shown in Fig. 10 indicates chemical exchange among three inequivalent carbons with relative intensity 2:2:1 [44]. Since the only way that carbons in three different sites can be interchanged is symmetry-equivalent reorientations of the C_{60}^{-3} unit, motional dynamics must be responsible for the spectral changes.

In principle, it should be possible to obtain correlation times and an activation energy for the reorientation of C_{60}^{-3} using dynamic NMR lineshape analysis techniques. This would require better resolution than we have obtained. The line broadening observed may be due to sample inhomogeneity leading to a distribution of isotropic chemical shifts; if this is the case, improvement of resolution will require the preparation of fresh samples. Alternatively, it may be possible to improve resolution by obtaining the data at higher field where the chemical shift spread is greater.

Acknowledgements

The skillful technical assistance of R. D. Kendrick is acknowledged. We thank Paul Bagus for help with hyperfine coupling calculations.

References

1 A. Dworkin, H. Szwarc, S. Leach, J. P. Hare, T. J. Dennis, H. W. Kroto, R. Taylor and D. R. M. Walton, *C.R. Acad. Sci. Paris, 312* (1991) 979–982.

2 A. Dworkin, C. Fabre, D. Schutz, G. Kriza, R. Ceolin, H. Szwarc, P. Bernier, D. Jérome, S. Leach, A. Rassat, J. P. Hare, T. J. Dennis, H. W. Kroto, R. Taylor and D. R. M. Walton, *C.R. Acad. Sci. Paris, 313* (1991) 1017–1021.
3 P. A. Heiney, J. E. Fischer, A. R. McGhie, W. J. Romanow, A. M. Denenstein, J. P. McCauley, Jr. and A. B. Smith III, *Phys. Rev. Lett., 66* (1991) 2911–2914.
4 R. Tycko, G. Dabbagh, R. M. Fleming, R. C. Haddon, A. V. Makhija and S. M. Zahurak, *Phys. Rev. Lett., 67* (1991) 1886–1889.
5 R. D. Johnson, C. S. Yannoni, H. C. Dorn, J. R. Salem and D. S. Bethune, *Science, 255* (1992) 1235.
6 Y. Maniwa, K. Mizoguchi, K. Kume, K. Kikuchi, I. Ikemoto, S. Suzuki and Y. Achiba, *Solid State Commun., 80* (1991) 609–612.
7 P. A. Heiney, G. B. M. Vaughan, J. E. Fischer, N. Coustel, D. E. Cox, J. R. D. Copley, D. A. Neumann, W. A. Kamitakahara, K. M. Creegan, D. M. Cox, J. P. McCauley, Jr. and A. B. Smith III, *Phys. Rev. B, 45* (1992) 4544–4547.
8 W. I. F. David, R. M. Ibberson, J. C. Matthewman, K. Prassides, T. J. S. Dennis, J. P. Hare, H. W. Kroto, R. Taylor and D. R. M. Walton, *Nature (London), 353* (1991) 147–149.
9 K. Prassides, T. J. S. Dennis, J. P. Hare, J. Tomkinson, H. W. Kroto, R. Taylor and D. R. M. Walton, *Chem. Phys. Lett., 187* (1991) 455–458.
10 D. A. Neumann, J. R. D. Copley, R. L. Cappelletti, W. A. Kamitakahara, R. M. Lindstrom, K. M. Creegan, D. M. Cox, W. J. Romanow, N. Coustel, J. P. McCauley, Jr., N. C. Maliszewskyj, J. E. Fischer and A. B. Smith III, *Phys. Rev. Lett., 67* (1991) 3808–3811.
11 W. I. F. David, R. M. Ibberson, T. J. S. Dennis, J. P. Hare and K. Prassides, *Europhys. Lett., 18* (1992) 219–225.
12 D. A. Neumann, J. R. D. Copley, W. A. Kamitakahara, J. J. Rush, R. L. Cappelletti, N. Coustel, J. P. McCauley, Jr., J. E. Fischer, A. B. Smith III, K. M. Creegan and D. M. Cox, *J. Chem. Phys., 96* (1992) 8631–8633.
13 R. F. Kiefl, J. W. Schneider, A. MacFarlane, K. Chow, T. L. Duty, T. L. Estle, B. Hitti, R. L. Lichti, E. J. Ansaldo, C. Schwab, P. W. Percival, G. Wei, S. Wlodek, K. Kojima, W. J. Romanow, J. P. McCauley, Jr., N. Coustel, J. E. Fischer and A. B. Smith III, *Phys. Rev. Lett., 68* (1992) 2708–2712.
14 S. H. Tolbert, A. P. Alivasatos, H. E. Lorenzana, M. B. Kruger and R. Jeanloz, *Chem. Phys. Lett., 188* (1992) 163–167.
15 P. H. M. van Loosdrecht, P. J. M. van Bentum and G. Meijer, *Phys. Rev. Lett., 68* (1992) 1176.
16 X. D. Shi, A. R. Kortran, J. M. Williams, A. M. Kini, B. M. Savall and P. M. Chaikin, *Phys. Rev. Lett., 68* (1992) 827–830.
17 R. D. Johnson, G. Meijer, J. R. Salem and D. S. Bethune, *J. Am. Chem. Soc., 113* (1991) 3619.
18 F. Diederich, R. Ettl, Y. Rubin, R. L. Whetten, R. Beck, M. Alvarez, S. Anz, D. Sensharma, F. Wudl, K. C. Khemani and A. Koch, *Science, 252* (1991) 548.
19 R. D. Johnson, C. S. Yannoni, J. R. Salem, D. S. Bethune, M. S. de Vries, C. A. Brown, H. R. Wendt and H. C. Dorn, *APS Abstr. Postdeadline Papers, Mar. Meet., Indianapolis, IN, USA, 1992.*
20 G. B. M. Vaughan, P. A. Heiney, J. E. Fischer, D. E. Luzzi, D. A. Ricketts-Foot, A. R. McGhie, Y. W. Hui, A. L. Smith, D. E. Cox, W. J. Romanow, B. H. Allen, N. Coustel, J. P. McCauley, Jr. and A. B. Smith III, *Science, 254* (1991) 1350–1353.
21 Y. Chai, T. Guo, C. Jin, R. E. Haufler, L. P. F. Chibante, J. Fure, L. Wang, J. M. Alford and R. E. Smalley, *J. Phys. Chem., 95* (1991) 7564–7568.
22 R. D. Johnson, M. S. de Vries, J. Salem, D. S. Bethune and C. S. Yannoni, *Nature (London), 355* (1992) 239.
23 C. S. Yannoni, M. Hoinkis, M. S. de Vries, D. S. Bethune, J. R. Salem, M. S. Crowder and R. D. Johnson, *Science, 256* (1992) 1191–1192.
24 G. Meijer, M. S. de Vries, H. R. Wendt and H. E. Hunziker, *Appl. Phys. B, 51* (1990) 395–403.

25 A. N. Shibanov, in V. S. Lethokov (ed.), *Laser Analytical Spectrochemistry*, Adam Hilger, Bristol, 1985.
26 *Handbook of Chemistry and Physics*, CRC Press, Boca Raton, FL, 72nd edn., 1991, pp. 12–18.
27 H. Shinohara, H. Sato, M. Ohkohchi, Y. Ando, T. Kodama, T. Shida, T. Kato and Y. Saito, *Nature (London), 357* (1992) 52–54.
28 R. E. Haufler, Lai-Sheng Wang, L. P. F. Chibante, Changming Jin, J. J. Conceicao, Yan Chai and R. E. Smalley, *Chem. Phys. Lett., 179* (1991) 449.
29 J. R. Heath, S. C. O'Brien, Q. Zhang, Y. Liu, R. F. Curl, H. W. Kroto, Q. Zhang, F. K. Tittel and R. E. Smalley, *J. Am. Chem. Soc., 107* (1985) 7779.
30 H. W. Kroto, J. R. Heath, S. C. O'Brien, R. F. Curl and R. E. Smalley, *Nature (London), 318* (1985) 162–163.
31 J. H. Weaver, Y. Chai, G. H. Kroll, C. Jin, T. R. Ohno, R. E. Haufler, T. Guo, J. M. Alford, J. Conceicao, L. P. F. Chibante, A. Jain, G. Palmer and R. E. Smalley, *Chem. Phys. Lett., 190* (1992) 460–464.
32 C. P. Poole, Jr., *Electron Spin Resonance: A Comprehensive Treatise on Experimental Techniques*, Wiley, New York, 2nd edn., 1983, p. 476.
33 J. R. Morton and K. F. Preston, *J. Magn. Reson., 30* (1978) 577–582.
34 A. Rosen and B. Waestberg, *Z. Phys. D, 12* (1989) 387–390.
35 R. C. Haddon, A. F. Hebard, M. J. Rosseinsky, D. W. Murphy, S. J. Duclos, K. B. Lyons, B. Miller, J. M. Rosamilia, R. M. Fleming, A. R. Kortan, S. H. Glarum, A. V. Makhija, A. J. Muller, R. H. Eick, S. M. Zahurak, R. Tycko, G. Dabbagh and F. A. Thiel, *Nature (London), 350* (1991) 320.
36 A. F. Hebard, M. J. Rosseinsky, R. C. Haddon, D. W. Murphy, S. H. Glarum, T. T. M. Palstra, A. P. Ramirez and A. R. Kortan, *Nature (London), 350* (1991) 600.
37 P. W. Stephens, L. Mihaly, P. L. Lee, R. L. Whetten, S.-M. Huang, R. B. Kaner, F. Diederich and K. Holczer, *Nature (London), 351* (1991) 632–634.
38 P. W. Stephens, L. Mihaly, J. B. Wiley, S.-M. Huang, R. B. Kaner, F. Diederich, R. L. Whetten and K. Holczer, *Phys. Rev. B, 45* (1992) 543–546.
39 R. Tycko, G. Dabbagh, M. J. Rosseinsky, D. W. Murphy, R. M. Fleming, A. P. Ramirez and J. C. Tully, *Science, 253* (1991) 884–886.
40 M. Kraus, J. Freytag, S. Gärtner, H. M. Vieth, W. Krätschmer and K. Lüders, *Z. Phys. B, 85* (1991) 1–2.
41 J. P. McCauley, Q. Zhu, N. Coustel, O. Zhou, G. Vaughan, S. H. F. Idziak, J. E. Fischer, S. W. Tozer, D. M. Groski, N. Bykovetz, C. L. Lin, A. R. McGhie, B. H. Allen, W. J. Romanow and A. M. Denenstein, *J. Am. Ceram. Soc., 113* (1991) 8537.
42 A. C. Hackmann, H. Seidel, R. D. Kendrick, P. C. Myhre and C. S. Yannoni, *J. Magn. Reson., 79* (1988) 148–153.
43 C. S. Yannoni, R. D. Johnson, G. Meijer, D. S. Bethune and J. R. Salem, *J. Phys. Chem., 95* (1991) 9.
44 J. Sandström, *Dynamic NMR Spectroscopy*, Academic Press, New York, 1982, Ch. 9.